ACS Catalysis

Research Article

pubs.acs.org/acscatalysis

Ab Initio Study of Thin Oxide–Metal Overlayers as an Inverse Catalytic System for Dioxygen Reduction and Enhanced CO Tolerance

Dongbin Shin,[†] S. Sinthika,[‡] Min Choi,[§] Ranjit Thapa,*[,‡] and Noejung Park*[,†,∥]

[†]Department of Physics, Ulsan National Institute of Science and Technology, Ulsan, 689-798 Korea

[‡]SRM Research Institute, SRM University, Kattankulathur 603203, Tamil Nadu, India

[§]Department of Chemistry, Ulsan National Institute of Science and Technology, Ulsan, 689-798 Korea

[∥]Center for Multidimensional Carbon Materials, Institute for Basic Science (IBS), Ulsan, 689-798 Korea

Supporting Information

ABSTRACT: Using first-principles density functional theory calculations, we used a thin oxide overlayer, such as MgO, on a metal surface as an inverse catalyst for dioxygen reduction. Surface distortions in the oxide layer, combined with the tunneling of electron from the underneath metal, activated the adsorbed O_2 in the form of a superoxo or peroxo. On the other hand, the thin MgO overlayer readily prevents the π-back-bonding between CO and the metal surface, thereby efficiently mitigating the affinity of the metal surface for CO. The operating potential and overpotential for the oxygen reduction reaction (ORR) process have been estimated for various combinations of thin insulators and metals. The strongest binding intermediate in the overall reaction pathway influenced the overpotential. We show that for a Ag(100)-supported MgO surface, the ORR commences with a low overpotential, which is comparable to that of the Pt(111) surface. This suggests that an optimally chosen insulator–metal overlayer structure can yield a sharply tuned free energy profile for ORR.

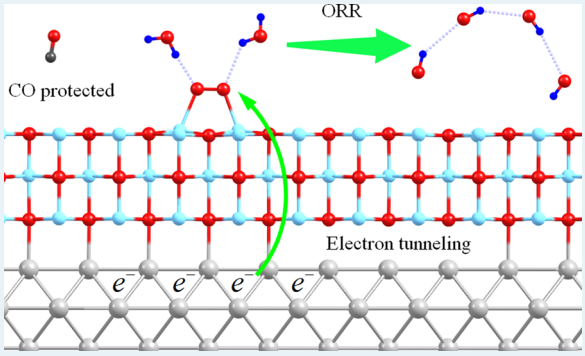

KEYWORDS: *ab initio calculation, electrocatalyst, inverse catalyst, overpotential, electron tunneling*

INTRODUCTION

The catalytic activities of solid surfaces for oxygen reduction or oxygen accompaniment reactions have been of great scientific significance for energy storage and conversion processes,[1−3] petrochemical engineering,[4] and environmental remediation through destroying the toxic radicals in flue gases.[5] For the purpose of being an ideal catalyst, the surface should provide sufficient binding affinity for O_2, with high durability against self-oxidation and lower likelihood of surface poisoning by the reactive species.[1,6,7] The d orbital states of metal surfaces have been considered the most pivotal element determining the efficiency of the catalyst.[8,9] On the other hand, the presence of unsaturated d orbital states on surfaces may provoke undesired strong binding of reactive partially oxidized species. For example, the strong binding of CO on a Pt surface, through a typical π-back-donation interaction, is most detrimental to the catalyst and is one of the main hurdles for the wide commercialization of low-temperature fuel cells, such as the proton exchange membrane fuel cell (PEMFC) and the direct methanol fuel cell (DMFC).[1,8,10,11]

To increase the CO tolerance of Pt catalysts, various systems have been tested, including alloying with transition metals (such as Ru) and fabrication of core–shell structures.[12−15] Catalysts based on non-metal elements, which are free of d electrons, have also been attractive, and a few recent studies have demonstrated an oxygen reduction reaction (ORR) using metal-free nanomaterials.[16,17] In terms of the reaction type, the direct four-electron reduction is greatly desired. The cathodic reaction for the cell of acidic media is $O_2 + 4H^+ + 4e^- \rightarrow 2H_2O$, and that of the alkaline cell is $O_2 + 2H_2O(l) + 4e^- \rightarrow 4OH^-$. The two-step sequential two-electron ORR pathway needs to be avoided as it can cause side reactions, leading to the formation of hydrogen peroxide (H_2O_2) that can damage carbon supports and is likely to retard the reaction kinetics.[18] A possible method for tuning the catalyst to achieve the direct four-electron reduction has been studied previously,[19] and it was shown that a modulation of the d orbital state can affect the formation of H_2O_2.[20]

In pursuit of improved catalytic activity and enhanced electrochemical stability, we are motivated to consider oxide–metal overlayer structures, as depicted in Scheme 1. This motivation originates from the observations of novel chemical

Received: August 8, 2014
Revised: October 4, 2014
Published: October 9, 2014

 © 2014 American Chemical Society dx.doi.org/10.1021/cs501153p | ACS Catal. 2014, 4, 4074−4080

Scheme 1. (a) Depiction of Catalysis of a Thin Oxide Overlayer on a Metal Surface and (b) an Example Model Geometry for Ag-Supported Three-Layer MgO and Adsorbed O_2 and Incoming Water Molecules

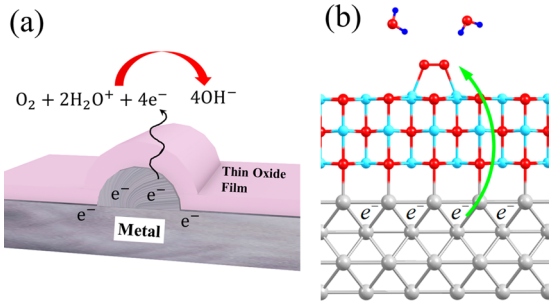

activity of atomically thin insulating oxide layers on a metal surface.[21,22] We mainly show in this work that if the oxide layer is in the range of possible electron tunneling from the metal surface, then a substantial portion of the oxide surface is catalytically effective. Thus, this model accounts for the catalytic activity of oxide nanoparticles supported on metal surfaces, which has been regarded as an inverse catalytic system, in contrast to the conventionally employed metal catalysts on oxide supports. A number of studies of inverse catalysts have demonstrated the performance of oxidation reactions like CO oxidation and the water gas shift reaction.[23,24] It has been reported that the electrons from the metal layer are readily available through tunneling; the insulating oxide surface can bind the electron-accepting species, such as NO_2, Au nanoclusters, and O_2.[21,22,25−30] On the other hand, the binding mechanism of CO is not based on the one-way charge transfer but relies on π-back-donation to the metal atom. This implies that the presence of a thin insulating overlayer on metal can sharply discriminate between the subtle differences in the adsorption chemistries of O_2 and CO: preventing the formation of π-back-bonding interaction while selectively allowing dixoygen adsorption and activation.

Besides CO tolerance, we also explored the ORR efficiency of oxide−metal overlayer structures through the calculations of the free energy profile along the ORR pathways. We show that the presence of a thin oxide overlayer can limit the overpotential. Among the studied combinations, the MgO on the Ag surface led to the smallest overpotential, which is comparable to that of the Pt(111) catalyst. In addition, the formation of H_2O_2 is highly unlikely on the thin insulator surface, because the dioxygen anion anchors on the surface with the two centers of thin insulator overlayers.

COMPUTATIONAL METHODS

We used the Vienna *Ab initio* Simulation Package (VASP).[31,32] A plane-wave basis set with an energy cutoff of 400 eV and the Perdew−Burke−Ernzerhof (PBE)-type gradient-corrected functional was used for the exchange-correlation potential.[33] The k-point meshes were sampled using the Monkhorst−Pack scheme. Atomic potentials were described with the Projector Augmented Wave (PAW) method, as provided with the aforementioned packages. The van der Waals (vdW) force was explicitly included using the DFT-D2 method to describe the noncovalent interlayer interactions between layered structures.[34]

RESULTS AND DISCUSSION

We first investigated adsorption energetics and the related electronic structures of CO binding to Pt(111) surfaces. Numerous previous studies have investigated CO adsorption on metal surfaces,[8,35] but here we summarize it to provide a direct comparison with the main content of this work. Figure 1a shows the potential energy curve of CO as a function of C−Pt distance. The energy at each point was calculated with a fixed C−Pt distance and with the other degrees of freedom being fully relaxed. Within the PBE density functional, CO adsorption on a Pt−Pt bridge was found to be slightly more stable than the adsorption on top of a Pt atom.[8] We found that the binding energies for the former case and the latter are 1.93 and 1.76 eV,

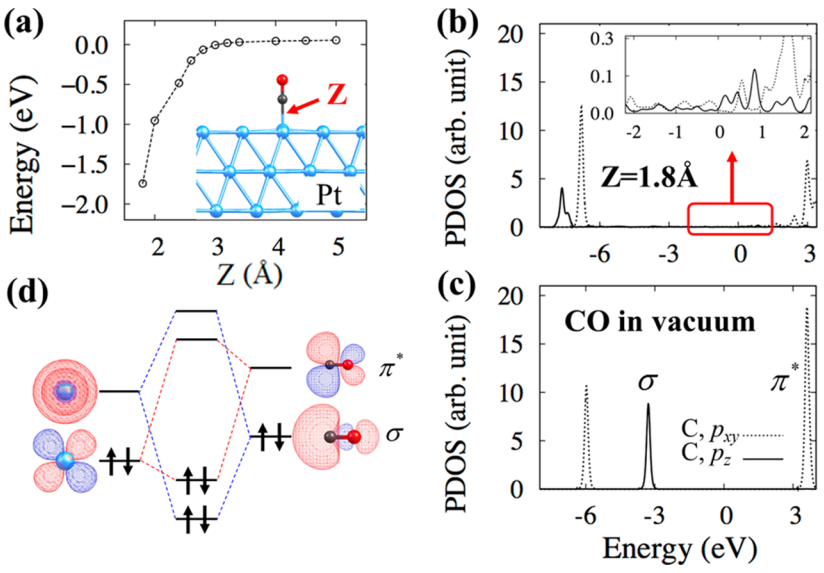

Figure 1. (a) Potential energy curve of CO on a Pt(111) surface as a function of C−Pt distance (Z). (b) PDOS for p_z and p_{xy} orbitals of C when CO adsorbs on top of a Pt (Z = 1.8 Å). The inset is the same PDOS in the close-up energy range. (c) PDOS for p_z and p_{xy} orbitals of C when CO in vacuum. (d) Schematic MO diagram for the formation of π-back-bonding between CO and Pt. In panel a, the red and dark gray spheres represent oxygen and carbon atoms, respectively. Larger steel blue spheres represent Pt atoms.

dx.doi.org/10.1021/cs501153p | *ACS Catal.* 2014, 4, 4074−4080

respectively. The adsorption paths for both configurations do not involve any energy barrier. As observed in various metal−ligand structures involving CO, the adsorption of CO on a Pt surface reveals the features of typical π-back-donation interactions. The PDOSs of p_z and p_{xy} orbitals of C of CO are presented in Figure 1b. For a clear comparison, the same PDOSs for p_z and p_{xy} orbitals of C, when CO is in the vacuum, are shown in Figure 1c, which explains that the highest occupied molecular orbital (HOMO) and the lowest unoccupied molecular orbital (LUMO) states of CO in vacuum are the σ and π^* states, respectively. Upon adsorption onto Pt, the hybridization of the HOMO and LUMO orbitals with Pt surface states induces up- and downshifts of the σ and π^* states, respectively, as shown in the inset of Figure 1b. A diagram of molecular orbital (MO) levels for such a π-back-donation interaction is depicted in Figure 1d.[8,35]

The strong bonding of CO on catalyst surfaces, as discussed in the previous paragraph, has been known to be the factor most detrimental to their catalytic efficiency. In this section, we show that the presence of a thin insulating overlayer effectively prevents the formation of the π-back-bonding interaction between CO and the metal surface. As an example, we first consider CO adsorption on Ag(100) with a thin MgO overlayer. In this computation, we used a (2 × 2) two-dimensional cell of three atom layers of MgO placed on the surface of a (2 × 2) supercell of Ag(100). Figure 2a shows the minimal energy configuration of the CO adsorbed on the MgO/Ag, in which the C of CO is bonded to Mg. We displaced CO along the z direction from the equilibrium position, and the calculated total energy of CO is shown in Figure 2b. For comparison, the same energy curve without Ag substrate is also presented. It is noteworthy that the binding of CO on the MgO/Ag shows features that are almost the same as those of CO on a MgO surface without the substrate metal (Figure 2b). The binding energy is 0.18 eV, within the PBE density functional calculation, and charge transfer is negligible, in agreement with the previous result.[36] This binding strength is slightly stronger than a usual intermolecular physisorption because of the polar interaction between MgO and CO.

The protection of metal against CO contamination can also be obtained by using another overlayer, such as graphene or hexagonal boron nitride (h-BN). As an example of the thinnest overlayer, we consider the h-BN monolayer on Pt(111) surfaces as shown in Figure 2c. In this computation, a $(2\sqrt{3} \times 4)$ supercell of a h-BN single layer on a $(3 \times 2\sqrt{3})$ supercell of Pt(111) constitutes the two-dimensional lattice with minimal lattice mismatch. The binding of CO to h-BN/Pt also reveals similar features, but the binding strength is weaker (0.04 eV) than in the MgO cases, as shown in Figure 2d. Again, the underneath metal layer has no influence on the binding of CO to h-BN, which is consistent with the previous results.[37−39]

The PDOSs for the p_z and p_{xy} orbitals of C, calculated at the equilibrium configuration of CO on MgO/Ag and h-BN/Pt, are presented in panels e and f of Figure 2, respectively. Like the CO in vacuum, the HOMO and LUMO states are the σ and π^* states, respectively, as signified by the p_z orbital and p_{xy} orbital states in the PDOSs presented in panels e and f of Figure 2, respectively. These PDOSs share the overall features of molecular CO in a vacuum, in sharp contrast to the π-back-bonding configuration presented in Figure 1c. Overall, the presence of a thin insulating layer efficiently blocked the π-back-donation interaction between CO and the metal surface.

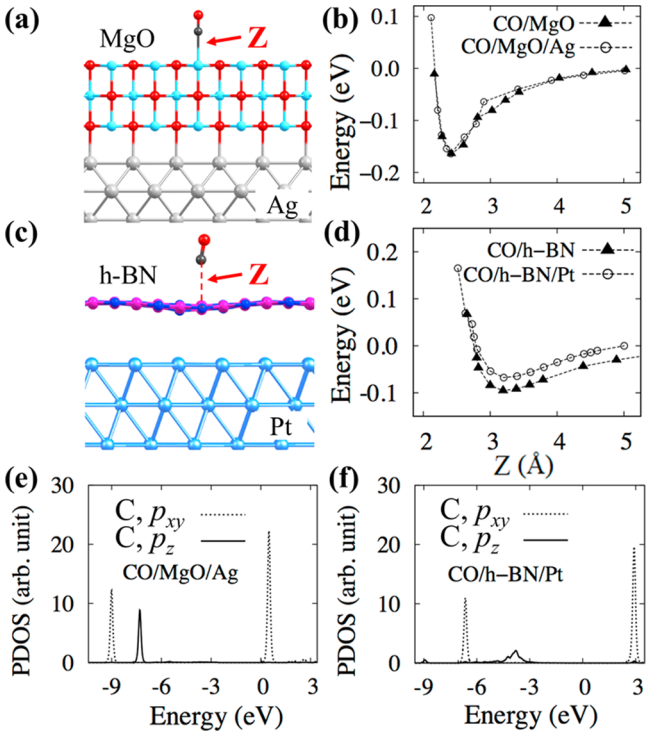

Figure 2. (a) Energy minimal configuration of CO adsorption on a thin MgO layer on Ag. (b) Potential energy of CO on the MgO surface with Ag and without Ag as a function of the nearest C−Mg distance. (c) Energy minimal configuration of CO adsorption on the h-BN monolayer on a Pt(111) surface. (d) Potential energy of CO on the h-BN surface with and without Pt as a function of the nearest C−B distance. (e and f) PDOS for p_z and p_{xy} orbitals of C when CO sits on the energy minimal configuration on MgO/Ag and h-BN/Pt. In panel a, the red, sky blue, and gray spheres represent oxygen, magnesium, and silver atoms, respectively. In panel c, pink and dark blue spheres represent boron and nitrogen atoms, respectively. Other atomic symbols are the same as those used in Figure 1.

While the binding of CO on a metal surface is due to the donation of a σ electron and back-donation of a π^* electron, the adsorption of dioxygen can be mostly attributed to one-way electron transfer from metal to O_2. Various forms of ligated metal atom can bind adsorbed dioxygen in either the "end-on" or "side-on" configuration, which can be related to the paramagnetic superoxo (O_2^-) or nonmagnetic peroxo (O_2^{2-}) state, respectively.[40−43] The adsorption state of such partially activated dioxygen adducts on solid surfaces has attracted much research. While the geometry of an undissociated dioxygen molecular anion on metal surfaces has been well understood, the charge state of O_2 on Pt surfaces has been debated. Qi et al. and Wang et al. suggested that the dioxygen adsorbed on a Pt−Pt bridge, which is thought to be the precursor to various dissociative chemisorptions, can be better described by a charge-neutral adsorption complex rather than peroxo or superoxo.[44,45] Similar neutral dioxygen adsorption complexes on other metal atoms or carbon nanotube surfaces were also discussed and identified as the singlet adsorption state of O_2.[46,47] Nevertheless, the adsorbed dioxygens on Pt surfaces show the features of activation with an elongated O−O bond length and thus can hardly be described as a neutral singlet adduct. For example, on the Pt−Pt bridge, the elongated O−O bond length is 1.36 Å, which corresponds to the O−O bond length of superoxo (O_2^-).

dx.doi.org/10.1021/cs501153p | ACS Catal. 2014, 4, 4074−4080

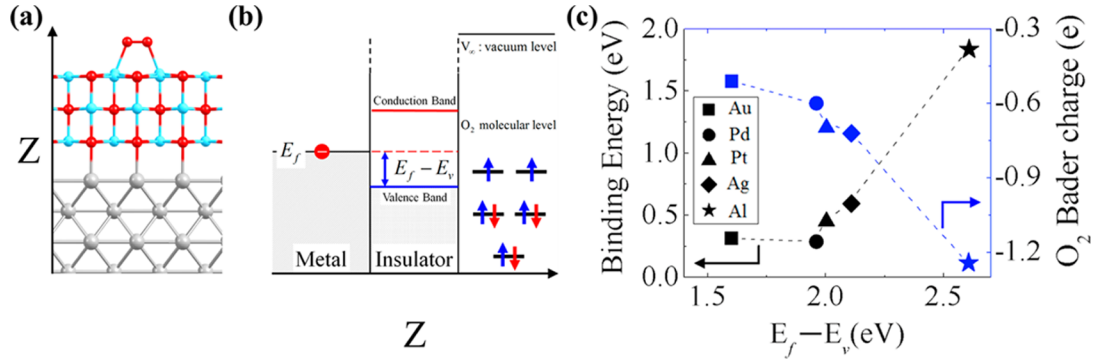

Figure 3. (a) Optimized geometry of adsorbed O_2 on a MgO/Ag surface. (b) Schematic energy diagram of the O_2/MgO/Ag system along the perpendicular (Z) direction. (c) Binding energy, Bader charge, and $E_f - E_v$ value of adsorbed O_2 on a MgO surface with various metal substrates. The up and down arrows in panel b represent the electron spin components. The dotted lines in panel c are guides to the eye. Atomic symbols are the same as those used in Figure 2.

Remarkably, thin oxide surfaces can bind such an activated dioxygen if an electron is supplied from a nearby metal.[25] Figure 3a shows the binding configuration of O_2 on the surface of a MgO layer on the Ag layer. The O−O bond length of the adsorbed dioxygen is 1.31 Å, which is 6.5% longer than that of triplet O_2 in vacuum. The O−O bond distance in the triplet O_2 in the vacuum is 1.23 Å upon calculation with the same density functional. This elongated bond length is an indication of dioxygen molecule transform as an anionic adduct. The schematic energy diagram is depicted in Figure 3b, emphasizing that the metal Fermi level is higher than the π^* state of O_2 to explain the electron transfer. Without the metal substrate and thus without electron transfer, the binding of O_2 on MgO is no more greater than the intermolecular physisorption. These features have been described well previously and are also depicted in Figure S1 of the Supporting Information.[21,25,26]

In this work, we investigated the effect of various choices of metal type. The charge and the binding of O_2 on the three-layer MgO slab, supported on various metals, are summarized in Figure 3c. The amount of transferred charge can naturally be related to the work function of the metal substrate. Another important effect is the dipole formed at the MgO−metal interface. The binding interaction between the metal surfaces with the bottom MgO layer depends on the detailed chemistry of each metal atom, and thus, metals with a similar work function can have different dipole strengths at the interface with MgO. However, the band alignment between the outer layer of MgO and the π^* state of the adsorbed dioxygen on the outer surface is thought to be almost fixed. Thus, instead of the work function of the bare metal surface, the height of the Fermi level with respect to the valence band maximum of MgO ($E_f - E_v$, as depicted in Figure 3b, is named the effective Fermi level hereafter) can be a better parameter for gauging the amount of charge transfer as a result of a combined effect including the dipole developed at the MgO−metal interface.

The MgO/Al interface shows the largest value in the effective Fermi level, which is mainly due to the smallness of the Al work function. Noticeably, Pt and Pd have effective Fermi level values larger than those of Au, even though the work function of bare Au is somewhat smaller than theirs. This can be attributed to the activity of Pt and Pd compared with that of the inert Au surface. The effective Fermi level of Au is even comparable to that of Ag. Figure 3c demonstrates that the amount of charge transfer (the charge of O_2) can be better correlated with the effective Fermi level than the bare work function. The more the charge transfers to the O_2 adsorbate, the stronger the bonding of O_2 on the MgO/metal surface. This trend again explains the Coulombic nature of the mechanism of binding between a dioxygen anion on the Mg cation and the surface. The aforementioned binding mechanism of O_2 can be applied to other thin insulators, such as h-BN. We also calculated similar dioxygen adsorption on single-layer h-BN with and without a supporting Al layer. We found that O_2 is activated and strongly adsorbs on h-BN only when it is supported on an Al layer. Our results are summarized in Figure S2 of the Supporting Information, which is consistent with the previous results of Ni-supported h-BN.[12,37]

In previous work, the efficiency of the catalyst for dioxygen reduction has been related to the adsorption mode of the undissociated dioxygen molecular anion.[48] The oxide−metal overlayers that can accommodate dioxygen molecular anions on the surface, as summarized in Figure 3c, can be utilized as a catalyst for dioxygen reduction. This model can be compared with the cerium oxide overlayer on metal that is known to be a good catalyst for the water−gas shift reaction.[49] We consider the free energy change along the ORR pathway on MgO on various metal surfaces. Realistic details of the microscopic phenomena at the liquid−solid interface in the ORR process are greatly challenging in the *ab initio* scheme.[50] Here we assume that "$H^+ + e^-$" is in equilibrium with $^1/_2H_2$, at pH 0 and 0 V versus the standard hydrogen electrode (SHE).[51,52] The one-electron reduction process is thought to be a coupled proton and electron transfer (CPET), and the applied potential is considered through a shift in the Fermi level of the electrode.[53] This approach allows us to shift the free energy value for intermediate steps by $-eU$, where U is the applied potential. Considering the known thermodynamic instability of oxides in acidic environments,[54] the calculations were performed assuming alkaline conditions, i.e., at pH 14, using the scheme described in the literature.[55] The equilibrium potential, which is commonly denoted U^0 in many studies, is hence 0.40 V versus the SHE. The free energy of water in the liquid phase was estimated as

$$G_{H_2O(l)} = G_{H_2O(g)} + RT \ln\left(\frac{p}{p_0}\right)$$

where R is the gas constant, T = 298.15 K, p = 0.035 bar, and p_0 = 1 bar. The free energy of O_2(g) was obtained as $G_{O_2(g)} = 2G_{H_2O(l)} - 2G_{H_2} - 4.92$ eV to balance the free energy under the

dx.doi.org/10.1021/cs501153p | ACS Catal. 2014, 4, 4074−4080

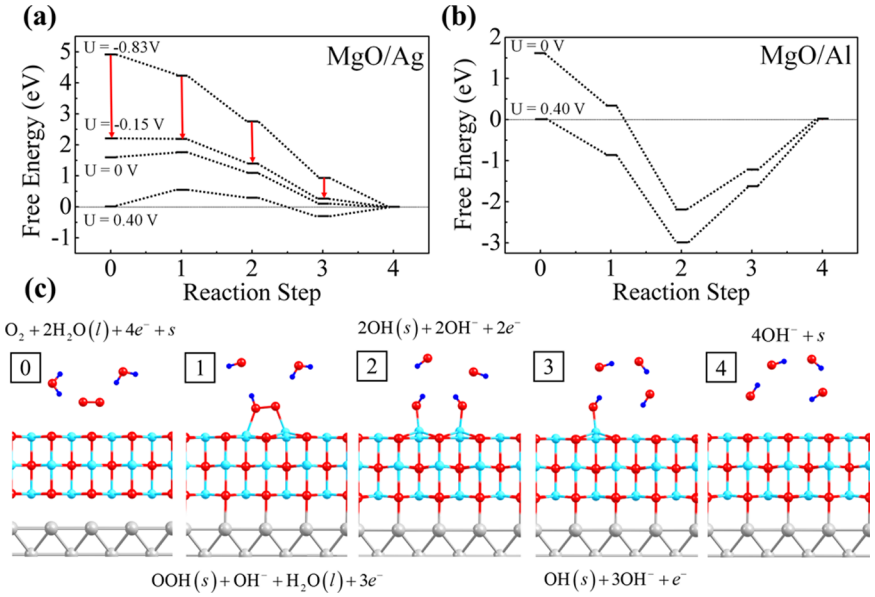

Figure 4. Free energy profile along the intermediate steps of the ORR in alkaline medium on the (a) MgO/Ag (100) and (b) MgO/Al (100) surfaces. (c) Atomic geometries and reaction formulas of each step. *U* represents the applied potential. The free energy considered for OH^- ion is derived separately in the text, and the free OH^- ions depicted in the subfigures are only for a better understanding. Blue spheres in panel c represent hydrogen atoms. All other atomic symbols are the same as those used in Figure 2. The dotted lines in panels a and b are guides to the eye.

aforementioned condition.[56] The free energy of the OH^- ion was derived as

$$G_{OH^-} = G_{H_2O(l)} - G_{H^+},$$

$$\text{where } G_{H^+} = \frac{1}{2}G_{H_2} - k_B T \ln 10 \times \text{pH}$$

In the alkaline medium, O_2 is reduced as $O_2 + 2H_2O(l) + 4e^- \rightarrow 4OH^-$, where the elementary reaction steps on the catalytic surface are

$$O_2 + 2H_2O(l) + 4e^- + s \rightarrow OOH(s) + OH^- + H_2O(l) + 3e^-$$

$$OOH(s) + OH^- + H_2O(l) + 3e^- \rightarrow 2OH(s) + 2OH^- + 2e^-$$

$$2OH(s) + 2OH^- + 2e^- \rightarrow OH(s) + 3OH^- + e^-$$

$$OH(s) + 3OH^- + e^- \rightarrow 4OH^- + s$$

where s denotes the free surface, X(s) denotes the active adsorption state of molecule X, and $H_2O(l)$ indicates liquid water. We note that the ORR using acidic medium also has similar reaction intermediates as considered in this study with the same number of protons and electrons transferred in each step. Thus, for a fixed potential on the reversible hydrogen electrode (RHE) scale, the free energy changes along the reaction pathways and the overall overpotential and operating potential are thought to be consistent irrespective of the type of electrolytic environment.[57]

The free energy change of each step in the reaction pathway can be defined as $\Delta G = \Delta E - T\Delta S - neU$, where ΔE represents the change in enthalpy (here, it was calculated from the DFT total energy) and ΔS is the change in entropy. Entropy change ΔS was obtained from a physical chemistry table, assuming H_2 and H_2O in gaseous form at room temperature and ambient pressure.[58] The entropy of the adsorbed state of the molecules is considered negligible compared to that of the gas phase.

We first examine the ORR reaction pathways on MgO/Ag and MgO/Al surfaces as shown in panels a and b of Figure 4, respectively (for the free energy profiles of other surfaces, see Figure S3 of the Supporting Information). The atomic geometries of the intermediate steps are shown in Figure 4c. At zero cell potential, the transfer of the first electron is uphill in energy on the MgO/Ag surface, while all other steps are exothermic. Upon adsorption, the oxygen molecule is attached to the surface in side-on fashion, anchored by two Mg atoms. The attachment of the first hydrogen requires an energy barrier of 0.15 eV. The second electron transfer step completely breaks the O−O bond, forming an intermediate with two OH groups attached to the surface (step 2 in Figure 4c). Notably, this step ensures that the additional adsorption of the second H does not lead to the development of H_2O_2. Subsequently, two more electron transfer steps result in the formation of $4OH^-$.

When the potential is corrected to the equilibrium potential of 0.40 V versus the SHE (1.23 V vs the RHE), the reaction energy for the first electron transfer increases to 0.55 eV. The second and third CPET steps occur exothermically, while the final desorption of OH(s) into OH^- experiences an easily surmountable thermodynamic barrier of 0.3 eV. The maximal potential at which all intermediate steps are downhill in the free energy profile (i.e., the operating potential) is hence estimated to be −0.15 V (0.68 V) with respect to the SHE (RHE). Hence, the formation of the OOH(s) intermediate is the rate-limiting step, requiring an activation barrier of ∼0.55 eV, which can be regarded as a measure of the overpotential. To comprehend the ORR activity of this catalyst, it is constructive to compare our results with those for the conventional Pt(111) surface. For the Pt (111) surface, the experimentally reported value of operating potential is <0.9 V.[53] Using the associative mechanism, we estimated the operating potential value to be ∼0.01 V (0.84 V) with respect to the SHE (RHE), and the overpotential is 0.39 V (for detailed ORR reaction steps on the

dx.doi.org/10.1021/cs501153p | ACS Catal. 2014, 4, 4074−4080

Pt(111) surface, see Figure S4 of the Supporting Information). The overpotential of a surface depends on the adsorption strength of the reaction intermediates. For an optimal ORR catalyst, the adsorption energy of the ORR intermediates should be neither too high nor two low. The overpotential is mostly determined by the strongest binding intermediates in the overall reaction pathway. Overall, the operating potential and the overpotential value of MgO/Ag are comparable to those of the Pt(111) surface. The only notable difference is that, for the Pt(111) surface, the last CPET step (i.e., OH desorption) is the rate-determining step, while the transfer of the first electron is the rate-limiting in the MgO/Ag surface.

Herein, we describe another example of the MgO shell on Al. This will help us understand the role of metals with different work functions on the catalytic property of the overlayer model catalyst. Figure 4b summarizes the free energy change along the reaction path for the MgO/Al surface at zero cell potential (U = 0 V) and at equilibrium potential (U = 0.40 V). We find that the final two steps are greatly uphill in energy at zero potential, and even at a reduced cell potential of −0.83 V (0 V vs the RHE), the activation energy is quite high, implying that the MgO/Al surface cannot be employed as an efficient catalyst for ORR.

We also investigated the possible paths for the formation of H_2O_2 on the MgO overlayer surfaces. The presence of H_2O_2 has been considered to be a main cause of the corrosion of the carbon support of the catalyst system. The transitions from adsorbed H_2O_2 to HOHO(s) on the Pt(111) surface were previously investigated, and the energy barrier to the dissociation of H_2O_2 was found to be 0.22 eV.[20] It is noteworthy that the same barrier to the dissociation of H_2O_2 on the MgO/Ag surface is negligible, which can be attributed to the fact that the adsorbed OH^- is more stable on the MgO/Ag surface because it is more electron-donating than the Pt(111) surface. As a result, the chance of forming H_2O_2 is reduced on this type of thin insulator−metal bilayer compare with that on a bare Pt surface, which can be an additional advantage for an optimized four-electron dioxygen reduction.

The realistic oxide surface can hardly be a perfect flat surface and can have oxygen vacancies or terraces. However, oxygen species, such as O_2 and H_2O, are actively involved in the ORR on the catalyst surface. Thus, the oxygen vacancy in the right front of the MgO surface can have a substantial chance of healing,[59,60] and thus, its effect over the ORR properties is thought to be minimal. This feature is discussed in Figure S5 of the Supporting Information along with the calculation of the ORR on the O-vacant MgO surface.

In summary, using first-principles density functional theory calculations, we investigated the adsorption chemistry of CO and O_2 on metal-supported thin insulator surfaces. We found that thin polar insulator surfaces, such as MgO or h-BN, can selectively activate O_2 in the form of a superoxo or peroxo state, through the concerted interplay of electron tunneling and polaron-like distortions on the insulator surface. On the other hand, the presence of atomically thin insulating overlayers readily prevents the π-back-bonding between CO and metal atoms, thereby efficiently mitigating the affinity of the metal surface for CO. The free energy profile of a various thin oxide overlayer on a metal surface indicates that the catalytic property and the value of overpotential can be tuned by changing the oxide−metal overlayer combination. The free energy change along the ORR process on the MgO/Ag layer revealed a very small value of the overpotential (0.55 eV), which is comparable to that of the Pt(111) surface. In addition, the presence of a thin insulator can modulate the oxidation tendency of metal surfaces such that even a metal with a small work function, such as Al, can optimally activate the O−O bond length that may lead to an acceptable dioxygen reduction process upon incorporation of protons.

■ ASSOCIATED CONTENT

Supporting Information

Electronic structures and optimized geometry of O_2 adsorbed on various thin insulator overlayers on a metal surface and free energy profiles of MgO/Pt, BN/Al, and Pt(111) surfaces. This material is available free of charge via the Internet at http://pubs.acs.org.

■ AUTHOR INFORMATION

Corresponding Authors

*E-mail: noejung@unist.ac.kr. Telephone: +82-52-217-2939. Fax: +82-52-217-3208.

*E-mail: ranjit.t@res.srmuniv.ac.in. Telephone: +91-44-2741-7918. Fax: +91-44-2745-6702.

Notes

The authors declare no competing financial interest.

■ ACKNOWLEDGMENTS

This research was supported by the Basic Science Research Program through the National Research Foundation of Korea (NRF), funded by the Ministry of Education (NRF-2013R1A1A2007910). This work was supported by IBS-R019-D1. R.T. thanks the Science and Engineering Research Board (SERB) of India for financial support (Grant SB/FTP/PS028/2013).

■ REFERENCES

(1) Winter, M.; Brodd, R. J. *Chem. Rev.* **2004**, *104*, 4245−4269.
(2) Debe, M. K. *Nature* **2012**, *486*, 43−51.
(3) Steele, B. C. H.; Heinzel, A. *Nature* **2001**, *414*, 345−352.
(4) Fierro, J. L. G. *Catal. Lett.* **1993**, *22*, 67−91.
(5) Ertl, G. *Angew. Chem., Int. Ed.* **2008**, *47*, 3524−3535.
(6) Wang, Y. X.; Balbuena, P. B. *J. Phys. Chem. B* **2005**, *109*, 14896−14907.
(7) Greeley, J.; Stephens, I. E. L.; Bondarenko, A. S.; Johansson, T. P.; Hansen, H. A.; Jaramillo, T. F.; Rossmeisl, J.; Chorkendorff, I.; Norskov, J. K. *Nat. Chem.* **2009**, *1*, 552−556.
(8) Hammer, B.; Morikawa, Y.; Norskøv, J. K. *Phys. Rev. Lett.* **1996**, *76*, 2141−2144.
(9) Hammer, B.; Norskøv, J. K. *Nature* **1995**, *376*, 238−240.
(10) Shao-Horn, Y.; Sheng, W. C.; Chen, S.; Ferreira, P. J.; Holby, E. F.; Morgan, D. *Top. Catal.* **2007**, *46*, 285−305.
(11) Ferreira, P. J.; la O', G. J.; Shao-Horn, Y.; Morgan, D.; Makharia, R.; Kocha, S.; Gasteiger, H. A. *J. Electrochem. Soc.* **2005**, *152*, A2256−A2271.
(12) Lyalin, A.; Nakayama, A.; Uosaki, K.; Taketsugu, T. *J. Phys. Chem. C* **2013**, *117*, 21359.
(13) Jiang, L.; Levchenko, S. V.; Rappe, A. M. *Phys. Rev. Lett.* **2012**, *108*, 166403.
(14) Iwasita, T.; Hoster, H.; John-Anacker, A.; Lin, W. F.; Vielstich, W. *Langmuir* **2000**, *16*, 522−529.
(15) Shen, S. Y.; Zhao, T. S.; Xu, J. B.; Li, Y. S. *J. Power Sources* **2010**, *195*, 1001−1006.
(16) Gong, K. P.; Du, F.; Xia, Z. H.; Durstock, M.; Dai, L. M. *Science* **2009**, *323*, 760−764.
(17) Qu, L. T.; Liu, Y.; Baek, J. B.; Dai, L. M. *ACS Nano* **2010**, *4*, 1321−1326.

(18) Markovic, N. M.; Schmidt, T. J.; Stamenkovic, V.; Ross, P. N. *Fuel Cells* **2001**, *1*, 105−116.
(19) Collman, J. P.; Devaraj, N. K.; Decreau, R. A.; Yang, Y.; Yan, Y. L.; Ebina, W.; Eberspacher, T. A.; Chidsey, C. E. D. *Science* **2007**, *315*, 1565−1568.
(20) Katsounaros, I.; Schneider, W. B.; Meier, J. C.; Benedikt, U.; Biedermann, P. U.; Auer, A. A.; Mayrhofer, K. J. J. *Phys. Chem. Chem. Phys.* **2012**, *14*, 7384−7391.
(21) Hellman, A.; Klacar, S.; Gronbeck, H. *J. Am. Chem. Soc.* **2009**, *131*, 16636.
(22) Pacchioni, G.; Giordano, L.; Baistrocchi, M. *Phys. Rev. Lett.* **2005**, *94*, 226104.
(23) Rodriguez, J. A.; Ma, S.; Liu, P.; Hrbek, J.; Evans, J.; Perez, M. *Science* **2007**, *318*, 1757−1760.
(24) Schoiswohl, J.; Surnev, S.; Netzer, F. P. *Top. Catal.* **2005**, *36*, 91−105.
(25) Pacchioni, G.; Freund, H. *Chem. Rev.* **2013**, *113*, 4035−4072.
(26) Gonchar, A.; Risse, T.; Freund, H. J.; Giordano, L.; Di Valentin, C.; Pacchioni, G. *Angew. Chem., Int. Ed.* **2011**, *50*, 2635−2638.
(27) Frondelius, P.; Hellman, A.; Honkala, K.; Hakkinen, H.; Gronbeck, H. *Phys. Rev. B* **2008**, *78*, 085426.
(28) Gronbeck, H. *J. Phys. Chem. B* **2006**, *110*, 11977−11981.
(29) Sterrer, M.; Risse, T.; Pozzoni, U. M.; Giordano, L.; Heyde, M.; Rust, H. P.; Pacchioni, G.; Freund, H. J. *Phys. Rev. Lett.* **2007**, *98*, 096107.
(30) Freund, H. J.; Pacchioni, G. *Chem. Soc. Rev.* **2008**, *37*, 2224−2242.
(31) Kresse, G.; Furthmüller, J. *Phys. Rev. B* **1996**, *54*, 11169−11186.
(32) Kresse, G.; Furthmüller, J. *Comput. Mater. Sci.* **1996**, *6*, 15−50.
(33) Perdew, J. P.; Burke, K.; Ernzerhof, M. *Phys. Rev. Lett.* **1996**, *77*, 3865−3868.
(34) Grimme, S. *J. Comput. Chem.* **2006**, *27*, 1787−1799.
(35) Miessler, G. L.; Tarr, D. A. *Inorganic chemistry*, 4th ed.; Pearson Prentice Hall: Upper Saddle River, NJ, 2011.
(36) Dovesi, R.; Orlando, R.; Ricca, F.; Roetti, C. *Surf. Sci.* **1987**, *186*, 267−278.
(37) Wasey, A. H. M. A.; Chakrabarty, S.; Das, G. P.; Majumder, C. *ACS Appl. Mater. Interfaces* **2013**, *5*, 10404−10408.
(38) Nigam, S.; Majumder, C. *ACS Nano* **2008**, *2*, 1422−1428.
(39) Ghosh, S.; Nigam, S.; Das, G. P.; Majumdar, C. *J. Chem. Phys.* **2010**, *132*, 164704.
(40) Tsuda, M.; Dy, E. S.; Kasai, H. *Eur. Phys. J. D* **2006**, *38*, 139−141.
(41) Cramer, C. J.; Tolman, W. B.; Theopold, K. H.; Rheingold, A. L. *Proc. Natl. Acad. Sci. U.S.A.* **2003**, *100*, 3635−3640.
(42) Nam, W. *Acc. Chem. Res.* **2007**, *40*, 465.
(43) Cho, J.; Sarangi, R.; Nam, W. *Acc. Chem. Res.* **2012**, *45*, 1321−1330.
(44) Qi, L.; Qian, X.; Li, J. *Phys. Rev. Lett.* **2008**, *101*, 146101.
(45) Wang, X. G.; Fisher, G. B. *Phys. Rev. Lett.* **2007**, *99*, 066101.
(46) Praetorius, J. M.; Allen, D. P.; Wang, R. Y.; Webb, J. D.; Grein, F.; Kennepohl, P.; Crudden, C. M. *J. Am. Chem. Soc.* **2008**, *130*, 3724−3725.
(47) Chan, S. P.; Chen, G.; Gong, X. G.; Liu, Z. F. *Phys. Rev. Lett.* **2003**, *90*, 086403.
(48) Lopez, N.; Norskøv, J. K. *J. Am. Chem. Soc.* **2002**, *124*, 11262−11263.
(49) Yang, F.; Graciani, J.; Evans, J.; Liu, P.; Hrbek, J.; Sanz, J. F.; Rodriguez, J. A. *J. Am. Chem. Soc.* **2011**, *133*, 3444−3451.
(50) Otani, M.; Sugino, O. *Phys. Rev. B* **2006**, *73*, 115407.
(51) Nørskov, J. K.; Rossmeisl, J.; Logadottir, A.; Lindqvist, L.; Kitchin, J. R.; Bligaard, T.; Jonsson, H. *J. Phys. Chem. B* **2004**, *108*, 17886−17892.
(52) Anderson, A. B.; Sidik, R. A.; Narayanasamy, J.; Shiller, P. *J. Phys. Chem. B* **2003**, *107*, 4618−4623.
(53) Keith, J. A.; Jacob, T. *Angew. Chem., Int. Ed.* **2010**, *49*, 9521−9525.
(54) Zhang, J. T.; Guo, C. X.; Zhang, L. Y.; Li, C. M. *Chem. Commun.* **2013**, *49*, 6334−6336.
(55) Jiao, Y.; Zheng, Y.; Jaroniec, M.; Qiao, S. Z. *J. Am. Chem. Soc.* **2014**, *136*, 4394−4403.
(56) Jones, R. O.; Gunnarsson, O. *Rev. Mod. Phys.* **1989**, *61*, 689−746.
(57) Su, H. Y.; Gorlin, Y.; Man, I. C.; Calle-Vallejo, F.; Norskov, J. K.; Jaramillo, T. F.; Rossmeisl, J. *Phys. Chem. Chem. Phys.* **2012**, *14*, 14010−14022.
(58) Atkins, P. W.; De Paula, J. *Physical chemistry*, 9th ed.; W. H. Freeman: New York, 2010.
(59) Ahlswede, B.; Homann, T.; Jug, K. *Surf. Sci.* **2000**, *445*, 49−59.
(60) Ealet, B.; Goniakowski, J.; Finocchi, F. *Phys. Rev. B* **2004**, *69*, 195413.